Contact Forces between Single Metal Oxide Nanoparticles in Gas-Phase Applications and Processes

Salameh, Samir; Van Der Veen, Monique A.; Kappl, Michael; Van Ommen, J. Ruud

DOI
10.1021/acs.langmuir.6b02982

Publication date
2017

Document Version
Final published version

Published in
Langmuir: the ACS journal of surfaces and colloids

Citation (APA)
Salameh, S., Van Der Veen, M. A., Kappl, M., & Van Ommen, J. R. (2017). Contact Forces between Single Metal Oxide Nanoparticles in Gas-Phase Applications and Processes. *Langmuir: the ACS journal of surfaces and colloids*, *33*(10), 2477-2484. https://doi.org/10.1021/acs.langmuir.6b02982

LANGMUIR

Article

pubs.acs.org/Langmuir

Contact Forces between Single Metal Oxide Nanoparticles in Gas-Phase Applications and Processes

Samir Salameh,*[,†] Monique A. van der Veen,[‡] Michael Kappl,[§] and J. Ruud van Ommen[†]

Delft University of Technology, [†]Department of Chemical Engineering, Product and Process Engineering, and [‡]Department of Chemical Engineering, Catalysis Engineering, 2628BL Delft, Netherlands

[§]Max Planck Institute for Polymer Research, Department of Physics at Interfaces, 55128 Mainz, Germany

Supporting Information

ABSTRACT: In this work we present a comprehensive experimental study to determine the contact forces between individual metal oxide nanoparticles in the gas-phase using atomic force microscopy. In addition, we determined the amount of physisorbed water for each type of particle surface. By comparing our results with mathematical models of the interaction forces, we could demonstrate that classical continuum models of van der Waals and capillary forces alone cannot sufficiently describe the experimental findings. Rather, the discrete nature of the molecules has to be considered, which leads to ordering at the interface and the occurrence of solvation forces. We demonstrate that inclusion of solvation forces in the model leads to quantitative agreement with experimental data and that tuning of the molecular order by addition of isopropanol vapor allows us to control the interaction forces between the nanoparticles.

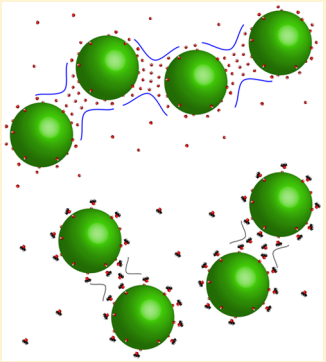

INTRODUCTION

Nanoparticles serve as the building block in an increasing amount of advanced materials and devices. Therefore, they are used in processes such as fluidization,[1,2] coating,[3,4] or mixing[5,6] to be implemented in products like gas sensors,[7] batteries,[8] or drug delivery systems.[9,10] In order to achieve best performance, it is crucial to have good control over the contact forces between the nanoparticles.[11−13] At the nanoscale, contact forces usually dominating over inertial forces and thus determine the interplay of individual nanoparticles.[14] They promote agglomeration of single nanoparticles, which explains why nanoparticles are rarely present individually.[15] On the one hand, individual nanoparticles would be advantageous for a lot of applications, on the other hand, also well-controlled degrees of agglomeration can be desired for certain applications. Hence, a fundamental understanding of the contact forces between single nanoparticles is necessary to achieve high-efficiently processes and high-quality products.

In general, contact forces are the summation of van der Waals, capillary, electrostatic, and double layer forces.[16,17] Since most of the industrial processes for nanoparticle synthesis are performed in the gas-phase,[18,19] this work focuses on contact forces between nanoparticles under ambient atmospheric conditions. Furthermore, it is questionable if state-of-the-art continuum theories sufficiently describe molecular interactions which become increasingly important at the nanoscale.[20,21] Therefore, we consider three possible forces: (i) van der Waals, (ii) capillary, and (iii) solvation. van der Waals forces between particles are generally described by the Hamaker approach.[22] The capillary force model depicts the formation of a liquid meniscus between two particles. Besides air humidity, the capillary force depends strongly on the macroscopic water contact angle of the material.[23] Finally, the solvation force predicts structuring of molecules between two opposite surfaces (e.g., particles). The molecules take discrete positions in the gap, leading to discrete energetically favorable gap distances.[24,25] In contrast to the Hamaker and capillary model, the solvation model is a noncontinuum approach. We analyze all experimentally determined contact forces in this work with regard to these three force models.

Measuring contact forces between nanosized objects is challenging. Typically, the atomic force microscope (AFM) is used.[21,26−32] This instrument measures the forces between a fine tip against an arbitrary substrate.[26,27] Multiple studies analyzed the acting forces between a single AFM-tip and flat surfaces and connected them to varying combinations of force models.[21,23,27−34] However, all these studies were limited to the tip−sample system without investigating real nanoparticles and did not use a coherent description of acting forces. Friedlander studied the mechanical behavior of nanoparticle agglomerates under strain with an AFM.[35,36] In a recent study, we pursued these investigations by detailed analyses of the measured forces. We showed that penetrating highly porous nanoparticle agglomerates with an AFM-tip is a reliable technique to measure contact forces directly between two individual nanoparticles. Parts of the agglomerate adhere to the AFM-tip. During retraction this parts unfold and finally detach at a particle−particle contact. Analyzing this particle−particle

Received: August 10, 2016
Revised: January 11, 2017
Published: February 10, 2017

DOI: 10.1021/acs.langmuir.6b02982
Langmuir 2017, 33, 2477−2484

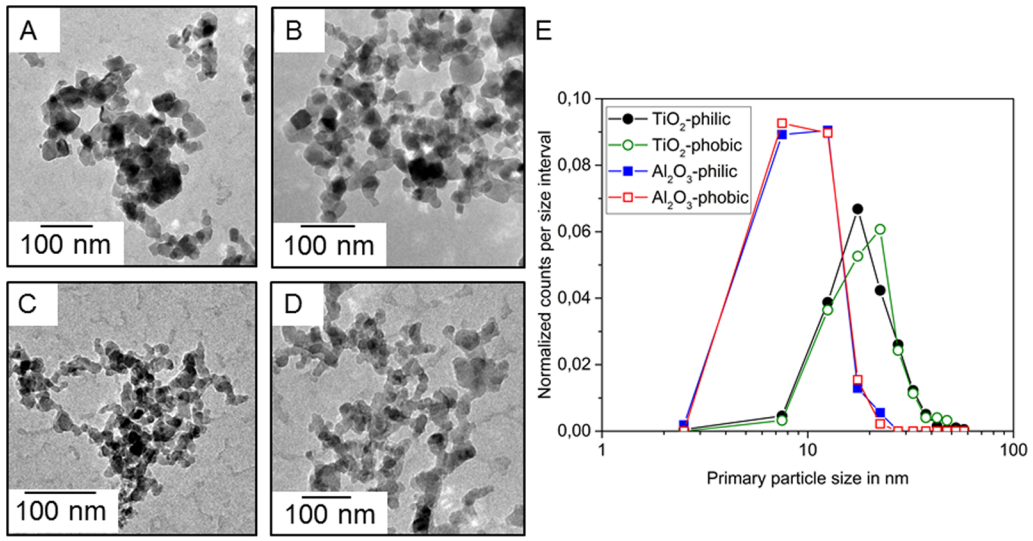

Figure 1. TEM analysis of TiO_2 and Al_2O_3. (A, B) TEM images of TiO_2-philic and TiO_2-phobic, respectively. (C, D) TEM images of Al_2O_3-philic and Al_2O_3-phobic, respectively. (E) TEM-based primary particle size distributions reveal no significant size differences based on the hydrophobization process.

breakage, our study suggested that contact forces between nanoparticles can be described by combination of capillary and solvation forces revealing the necessity to consider non-continuum effects.[20,37−39] However, the measurements were focused on hydrophilic TiO_2 nanoparticles, and therefore, the influence of key properties such as material, surface, and environment has to be proven for a general implementation. So far, no accurate characterization of the contact forces between two individual nanoparticles is available in the literature.

This paper elucidates the major interparticle forces between metal oxide nanoparticles in the gas-phase based on force spectroscopy. We show that these forces can be explained by a combination of capillary and solvation forces. To highlight the importance of surface properties and to show the general validity of our force concept, we analyze systematically two different metal oxides. We then propose a mathematical description which calculates the contact forces in agreement with our experimental results.

EXPERIMENTAL SECTION

Particle Characterization. In this study, industrially made TiO_2 and Al_2O_3 nanoparticles (Evonik industries) were analyzed. Both materials were purchased in two surface variations, hydrophilic and hydrophobic. The hydrophobic surfaces were achieved by hydrophobization of the hydrophilic nanoparticles.[40] The primary particle size distributions were analyzed in a Joel 1400 TEM in vacuum of 10^{-5} mbar and a voltage of about 120 kV. Further, the infrared spectra of the nanopowders were obtained by Diffuse Reflectance Infrared Fourier Transform spectroscopy (DRIFT) measurements using a IF566 spectrometer (Bruker) equipped with a praying mantis accessory and a temperature reaction chamber (Harrick). The samples were heated up to 120 °C for 1 h in helium environment to remove the physisorbed water and study the OH surface group structure. Also, TGA analysis was performed on all four powders. The powders where heated up from 20 to 120 °C with 10 °C/min, 10 min break at 120 °C, and then to 700 °C with 20 °C/min in a nitrogen atmosphere to quantify the amount of physisorbed water and OH surface groups based on the work of Mueller.[41]

Force Measurements. Nanopowders were cautiously heaped up onto a double-sided tape on a microscope slide. Then the microscope slide was knocked off to remove loosely bounded agglomerates. This procedure was repeated three times for every sample to achieve a homogeneous distribution of nanoparticle agglomerates in the size range of a few hundred μm onto the double-sided tape.[39]

Atomic force microscope measurements were taken in a Nanowizard 3 (JPK) using triangular Si_3N_4 cantilever (DNPS from Bruker). The AFM was mounted onto a vibration isolation table (i4 from Accurion) in a noise isolation box (JPK). Force measurement were performed under ambient conditions (temperature ∼20 °C and humidity ∼50%). The spring constant of the cantilever were 0.14 N/m and determined with the thermal noise method on a cleaned microscope glass slide.[42] Nanoparticle agglomerates was selected by a top view camera mounted on the AFM. Then 64 force curves were recorded using force mapping mode within an 8 × 8 grid over an area of 2 × 2 μm. This procedure was repeated multiple times on different agglomerates to average local inhomogeneity's and collect between 250−450 force curves for each single sample. The applied force was between 2.5 and 5 nN and the cantilever speed was fixed to 2 μm/s for every sample. The measured contact force between two single nanoparticles was determined by a statistical analyses of the last peak in the corresponding force curves, as described in detail in ref 20.

RESULTS AND DISCUSSION

Characterization of Nanopowders. Since surface properties strongly influence the strength of acting contact forces we investigate two different metal oxides of general interest, TiO_2 and Al_2O_3.[16] Both materials where chemically treated by the manufacturer leading to two surface modifications of each material. The Brunauer−Emmett−Teller (BET) diameter is given from the supplier and based on nitrogen adsorption−desorption measurements.

To analyze the primary particle sizes, Figure 1A−D shows the TEM images for TiO_2-philic, TiO_2-phobic, Al_2O_3-philic, and Al_2O_3-phobic, respectively.

The obtained primary particles distributions (Figure 1E) were fitted by log-normal distributions (fits are not shown) which showed the best fits and are in good agreement with the literature.[43] The calculated maxima of the fitted distribution were 9, 10, 17, and 18 nm for hydrophilic and hydrophobic alumina and hydrophilic and hydrophobic titania, respectively. Compared to the BET values (see Table 1), the obtained values are about 3−4 nm smaller. However, this discrepancy is based on the single measurement techniques as already reported in 44. The TEM analysis reveals no change in primary particle size

DOI: 10.1021/acs.langmuir.6b02982
Langmuir 2017, 33, 2477−2484

Table 1. Used Nanopowders Based on Supplier Information

signature	material	surface type	d_{BET} in nm
TiO_2-philic	TiO_2	hydrophilic	21
TiO_2-phobic	TiO_2	hydrophobic	21
Al_2O_3-philic	Al_2O_3	hydrophilic	13
Al_2O_3-phobic	Al_2O_3	hydrophobic	13

due to surface treatment. Therefore, no change in particle morphology is assumed which is supported by qualitative analyses of the TEM images (Figure 1A–D).

For all considered contact force models the structure of the surface is very important. The amount of OH-surface groups determines the physisorption of water molecules. This influences the materials Hamaker constant A_H, the contact angle θ, and the structuring of the water molecules on the particle surfaces.[16,17] Therefore, the nanoparticles surfaces are comprehensively analyzed by DRIFT (Figure 2) and thermogravimetric analysis (TGA/Figure 3) measurements.

The DRIFT measurements reveal the composition of the surfaces of the different materials. Based on the high temperatures (120 °C) during the measurements physisorbed water (3400–3600 1/cm) diminishes for TiO_2, while Al_2O_3 still shows the presence of water molecules on the surface. However, the OH surface groups between 3600–3800 1/cm (peak for TiO_2 and small shoulder for Al_2O_3) can be identified for both hydrophilic materials while the peaks are not present for the hydrophobic versions of the materials (Figure 2). These results are in good agreement with an earlier FTIR/XPS study where Erdem et al. reported that the number of OH surface groups reduces from 3,3 #/nm^2 for TiO_2-philic to 1.8 #/nm^2 for TiO_2-phobic.[45] Since DRIFT measurements are not able to quantify the exact amount of OH groups per area, TGA analyses were performed on all four powders.

The TGA measurements were normalized to the weight at 120 °C to distinguish between physisorbed water and OH surface groups, as described in detail by Mueller et al.[41] Based on this method the amount of OH surface groups can be calculated with the weight loss above 120 °C for the hydrophilic powders. The hydrophobic powders show a much larger weight loss above 120 °C since both, OH surface groups and organic molecules from the hydrophobization process desorb. A distinction between the OH groups and the organics was not possible. For the hydrophilic nanoparticles a value of 6,4 #/nm^2 and 11 #/nm^2 for TiO_2 and Al_2O_3 are obtained,

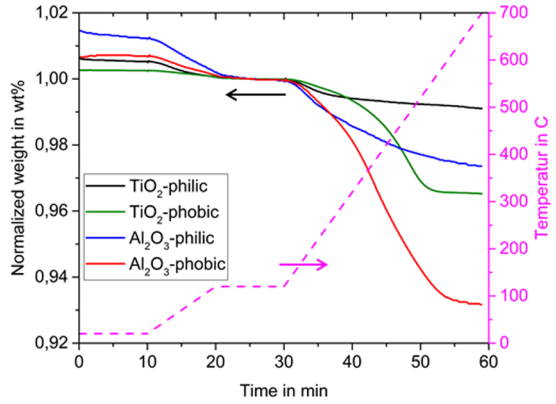

Figure 3. TGA analysis shows an OH surface density of 6.4 and 11 #/nm^2 for hydrophilic TiO_2 and Al_2O_3. The amount of physisorbed water is decreased for the hydrophobic counterparts.

which is in good agreement with earlier studies.[41] Furthermore, the TGA reveals that the hydrophilic nanoparticles carry more physisorbed water than the hydrophobic ones before the temperature treatment. However, it is obvious that even in pure N_2 atmosphere, all four powders carry a noticeable amount of water which only disappears by increasing the temperature. This was confirmed by DRIFT measurements at room temperature (see Figure S1, Supporting Information).

AFM Force Measurements between Single Nanoparticles. To analyze the contact forces between two individual nanoparticles, AFM force spectroscopy was performed on all four powders (ambient conditions) by penetrating highly porous agglomerates with the AFM tip and extract single chains of nanoparticles, as described in the methods. Figure 4 shows selected force curves for hydrophilic titania (A) and hydrophobic alumina nanoparticle agglomerates (B; for more data, see Figures S2 and S3, Supporting Information). During approach the AFM-tip pierces into the agglomerate while nanoparticles are pushed away and rearrange as shown by the peaks in the approach curve.[20,39] During retraction, nanoparticles stick to the tip and bridge the tip with the agglomerate. The chain between the tip and the agglomerate unfolds by rearranging, rolling/sliding, and breaking bonds between the nanoparticles explaining the multiple peaks in the force curve. While the first peaks contain information on multiple nanoparticles in contact, we recently

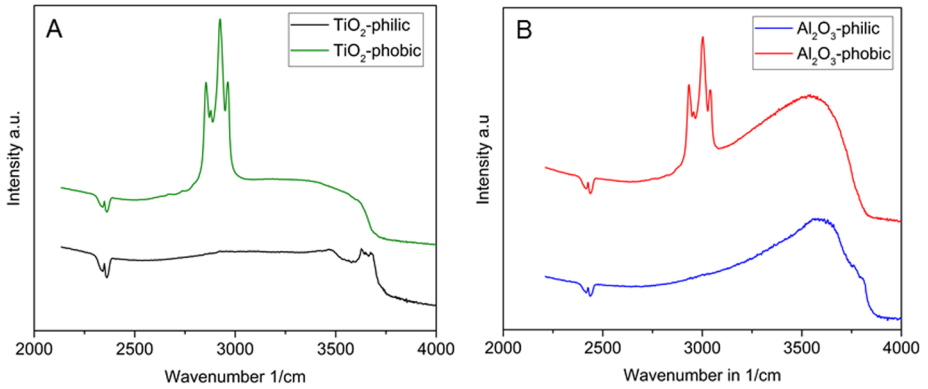

Figure 2. DRIFT measurements at 120 °C show the presence of hydroxyl groups for both hydrophilic materials. For the hydrophobic materials the amount of hydroxyl groups is clearly reduced (peaks at 3600–3800 1/cm). Further, the presence of hydrophobic groups, namely aliphatic C–H bonds, for hydrophobic TiO_2 and Al_2O_3 between 2800 and 3000 1/cm is obvious.

DOI: 10.1021/acs.langmuir.6b02982
Langmuir 2017, 33, 2477–2484

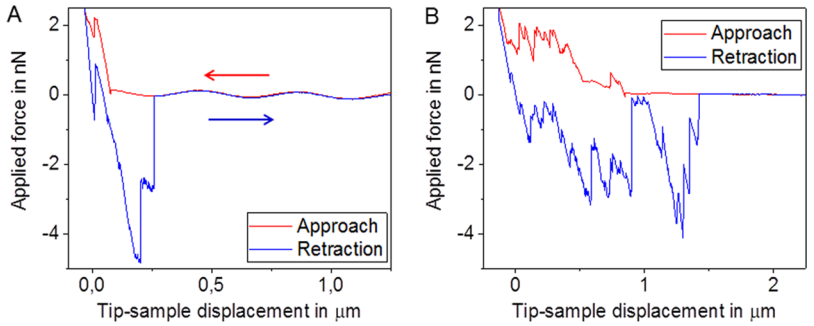

Figure 4. Force curves of hydrophilic titania (A) and hydrophobic alumina (B) nanoparticle agglomerates. The agglomerates first unfold and finally break at two individual nanoparticles in contact. The last peak (F_c) refers therefore to the contact force between two individual nanoparticles.

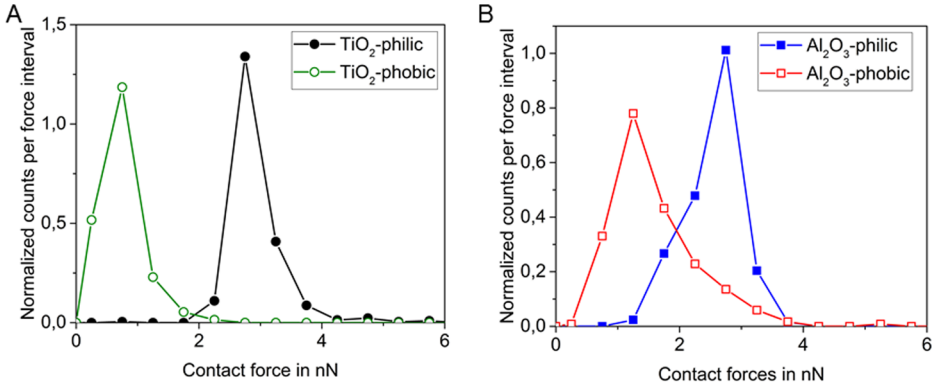

Figure 5. (A) Force distributions of the contact force between hydrophilic and hydrophobic titania nanoparticles obtained from the last peak of the measured force curves. (B) Force distribution of the contact force between hydrophilic and hydrophobic alumina nanoparticles. The hydrophobic nanoparticles show much lower contact forces than their hydrophilic counterparts. This trend is less prominent for alumina based on the larger amount of OH-surface groups and physisorbed water.

showed that the last peak can be related to the breakage of the bond between two individual nanoparticles (for clarification, see also Figure S4 in the Supporting Information).[20,38] Therefore, we focus in this study only on the measured contact force between two individual nanoparticles obtained from the last peak (F_c).

A statistical analysis of the last peak (F_c) can give fundamental inside into the acting contact forces between two individual nanoparticles. Therefore, Figure 5 shows normalized contact force distributions obtained from force curves measured on TiO_2 and Al_2O_3 with and without surface modifications.

In the case of TiO_2, the distributions show a log-normal behavior which is in good agreement with previous measurements.[20] The maximum of the distribution for the hydrophobic TiO_2 is at 0.5 nN and for the hydrophilic TiO_2 at 2.8 nN. For Al_2O_3 the maximum of the hydrophobic nanoparticles is at 1.2 nN, while the force increases again for the hydrophilic to 2.7 nN. The TiO_2 force distributions show a significant difference while the distributions overlap to a certain extent in the case of Al_2O_3. The surface characterization revealed that all particles carry a certain amount of physisorbed water. This amount of water corresponds to a layer of 1−2 nm high; so about 1 order of magnitude smaller than the particle diameter (2−40 nm). In earlier studies we already showed by AFM force measurements and all atom Molecular Dynamics simulations that contact forces between hydrophilic TiO_2 nanoparticles in the size range of ∼10 nm can be described by a combination of capillary and oscillating forces (solvation forces).[20,37] Therefore, we think that two individual metal oxide nanoparticles interact via a network of water molecules between them. This network is much weaker for hydrophobic particles leading to decreased contact forces. However, the hydrophobic Al_2O_3 nanoparticles still carry a noticeable amount of physisorbed water (see Figures 2 and 3), explaining why the force difference is less-pronounced compared to TiO_2. The interaction via this water molecule network further explains the generally strong measured forces for Al_2O_3. Based on Figure 1, the Al_2O_3 nanoparticles are much smaller compared to TiO_2 and contact forces scale with particle size.[14] However, the large amount of OH-surface groups and physisorbed water on the smaller Al_2O_3 nanoparticles explain why the measured contact forces are in the same size as for the larger TiO_2 nanoparticles. Recent studies show that the structuring of water molecules and oscillating forces have to be considered for a correct description of water menisci on the scale of a few nanometer.[46−49] However, direct measurements of oscillating forces in a chain of nanoparticles using an AFM is very challenging because of the "jump-out" problem. When the applied force exceeds the spring constant of the cantilever the tip jumps away from the sample. Using a stiffer tip would avoid this problem but decrease the sensitivity of the measurement.[46] Therefore, theoretical or computational approaches have to be used to analyze the details in the last peak (F_c). Capillary, as well as solvation forces, strongly depend on the physisorbed water.[16,17] In the case of hydrophilic nanoparticles, OH-surface groups enhance the physisorption of water (see Figures 2 and 3). This leads to a stronger capillary as well as a more structured ensemble of water molecules in the gap between the particles, while for hydrophobic particles both effects are less pronounced.

DOI: 10.1021/acs.langmuir.6b02982
Langmuir 2017, 33, 2477−2484

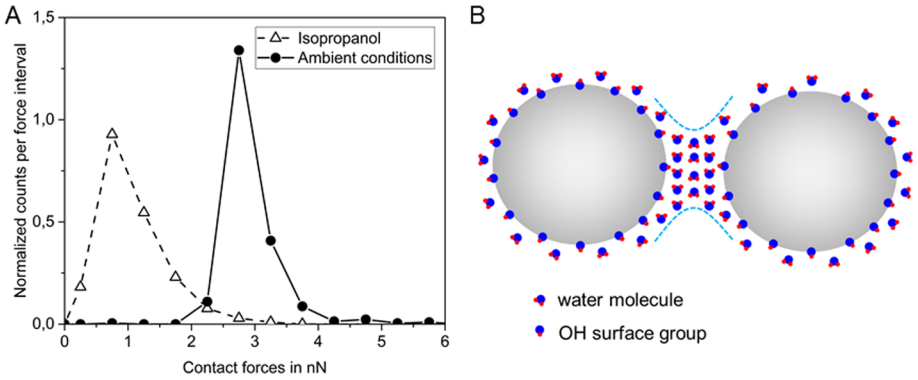

Figure 6. (A) Force distribution for TiO_2-philic under ambient conditions and in isopropanol atmosphere. The presence of isopropanol leads to a shielding of the polar interactions based on the weaker molecular interactions. (B) Schematic depiction of two interacting nanoparticles. Physisorbed water molecules structure between the nanoparticles leading to the formation of a liquid meniscus (dashed blue lines).

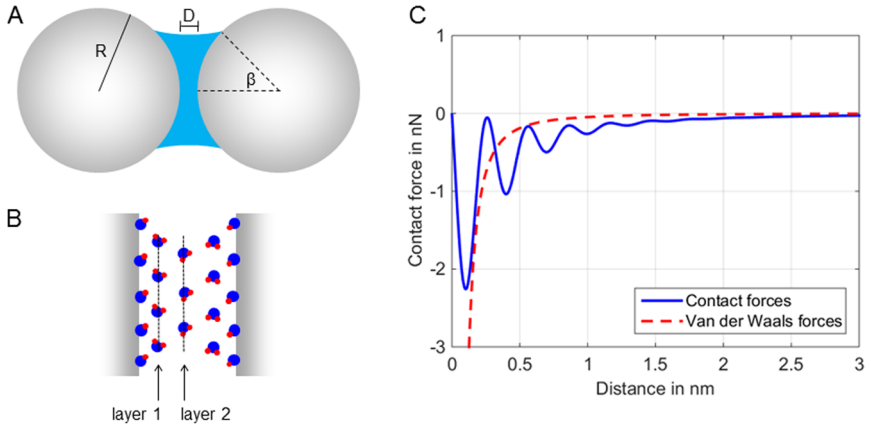

Figure 7. Calculation of the contact forces between two TiO_2 nanoparticles in the size 10 nm using macroscopic capillary forces (A) and noncontinuum solvation forces (B). Comparison to the state-of-the-art van der Waals model shows the necessity to consider noncontinuum effects.

However, describing the molecular interactions by the solvation force model directly excludes the macroscopic van der Waals model, which is typically used to describe the contact forces between particles.[50,51] Both models use the van der Waals interaction between single molecules as a basis. While the macroscopic van der Waals model is a simple pairwise add up of these interactions the solvation force model considers the discrete positions and structures of the interacting molecules. Furthermore, the macroscopic van der Waals model would predict a decreased force for the smaller Al_2O_3 particles compared to TiO_2 since their Hamaker constants are similar, which contradicts the measured results.[52,53]

To further prove the influence of physisorbed molecules on the contact forces, AFM experiments with TiO_2-philic were repeated under enriched isopropanol atmosphere.

In the presence of isopropanol the contact forces decrease from a maximum of 2.8−0.7 nN (Figure 6A), which is comparable to the measured differences between hydrophilic and hydrophobic nanoparticles (Figure 5A). Based on the stated picture of contact forces (Figure 6B), the amphiphilic isopropanol molecules physisorbed onto the particle surfaces. While the polar part directly connects with the OH surface groups, the apolar parts act as an hydrophobic coating weakening the water network between the particles. Therefore, the interaction force is lower compared to hydrophilic TiO_2 at ambient conditions. This influence of isopropanol on contact forces was already reported on a macroscopic scale during fluidization of oxide nanoparticles.[1] A comparison to the macroscopic van der Waals model again leads to different results. Since the Hamaker constant does not decrease in the presence of isopropanol, the calculated force stays the same.[54]

Mathematical Description of the Contact Forces. To test the hypothesis derived from the literature that contact forces between individual metal oxide nanoparticles can be described by a combination of capillary and solvation forces we develop a mathematical model ($F_c = F_{cap} + F_{sol}$) and compared it to the state-of-the-art van der Waals model. Capillary force F_{cap} is calculated by the means of the continuum model for two equal spheres (Figure 6A).[16]

$$F_{cap} = -\pi\gamma R(\cos(\theta + \beta) + \cos(\theta))\left(1 - \frac{D}{\sqrt{\frac{V}{0.5\pi R} + D^2}}\right) \quad (1)$$

Here R is the particle radius, θ the contact angle, β describes the position of the three-phase contact line, γ is surface tension, V is the volume of the meniscus assumed to be constant, and D is the interparticle distance. All used values are listed in Table S1 in the Supporting Information. The validity of this macroscopic approach for nanoparticles is questionable. However, the adjustment of the continuum capillary model for nanoparticles is still object of a strong debate.[28,30,55−58] Since correct values for θ, γ, or the validity of a circular meniscus is not well understood for nanoparticles so far, we

DOI: 10.1021/acs.langmuir.6b02982
Langmuir 2017, 33, 2477−2484

prefer to use a simple and verifiable model to describe the meniscus force.

The solvation force F_{sol} (Figure 6B) is calculated by eq 2 based on the work of Horn et al.[24] and adapted for two spherical particles.

$$F_{sol} = 0.5Rf_0 \frac{1}{\sqrt{\frac{1}{(2\pi\lambda)^2} + \frac{1}{d_0^2}}} e^{-D/\lambda} \cos\left(\frac{2\pi D}{d_0} + \Phi\right) \quad (2)$$

λ is the decay length and d_0 the layer thickness. Both values are assumed to be equal to the molecule size.[16] Φ is a phase shift and f_0 is the amplitude of the first maximum normally regarded as a fitting parameter, while we obtained a correct value from MD simulations of TiO_2 nanoparticles in bulk water.[37] For a more detailed description of eq 2, see Supporting Information.

The van der Waals forces are described by the means of the standard Hamaker model:[22]

$$F_{vdw} = \frac{A_H R}{12D^2} \quad (3)$$

with A_H being the Hamaker constant. Figure 7C shows the calculation for the contact forces over distance compared to the outcome of the van der Waals model.

Figure 7C shows an oscillating contact force with multiple force minima. These force minima depend on the energetically favorable structure of the molecules between the particles. The maximum contact force of the first minima at 2.3 nN is in very good agreement with the measured values for hydrophilic titania (see Figure 5 A). The decreasing oscillating force coincides with the predictions from earlier MD simulations for two TiO_2 nanoparticles.[20,37] Therefore, combining capillary and solvation forces is a promising approach to explain the contact forces between individual nanoparticles in the range of tens of nanometers. The macroscopic van der Waals model (using A_H for water) fails to describe the correct physics between the nanoparticles since the molecular structuring is not considered. However, the van der Waals force strongly depends on the interparticle distance D, which is generally assumed to be in the order of 0.3 nm.[17] Since Figure 7 C shows that F_{vdw} and F_C are about equal at the position of the first minima (D = 0.1 nm), the F_{vdw} approach could be used for an easy estimation of contact forces. Nevertheless, this distance has to be determined for each single system, which is challenging and needs complex MD simulations. Therefore, the mathematical approach based on F_{cap} + F_{sol} is the more easy and correct way to calculate acting contact forces between individual nanoparticles.

CONCLUSIONS

In this work we experimentally analyzed the contact forces between individual oxide nanoparticles in the gas-phase. We demonstrated by means of force spectroscopy measurements that contact forces between two nanoparticles can be explained by a water molecule network between the nanoparticles. This network can be described by a combination of capillary and solvation forces. In detail, a meniscus is formed between two particles based on the physisorbed water molecules. The molecules take discrete positions within the meniscus elucidating the fact that noncontinuum effects have to be considered to correctly describe the interplay between the nanoparticles. Our results show that these forces can easily be manipulated by making use of the molecular interaction between the nanoparticles. Finally, a mathematical model was developed combining capillary and solvation forces and was in very good agreement with the experimental results and earlier MD simulations. However, the full picture is by far not understood, and future work should concentrate on the surface characterization of nanostructures. Especially, the physisorption and structuring of molecules on particle surfaces is of great interest. We think that these results will have a strong impact on the field of contact forces between nanostructures and processing of nanoparticles, since adhesion effects are so commonly described using state-of-the-art continuum theories.

ASSOCIATED CONTENT

Supporting Information

The Supporting Information is available free of charge on the ACS Publications website at DOI: 10.1021/acs.langmuir.6b02982.

Figure S1−S4, Table S1, and eqns SI-1−SI-5, as well as supporting references (PDF).

AUTHOR INFORMATION

Corresponding Author

*E-mail: s.salameh@tudelft.nl.

ORCID

Samir Salameh: 0000-0002-8986-3958

Notes

The authors declare no competing financial interest.

ACKNOWLEDGMENTS

The research leading to this paper has received funding from the European Research Council under the European Union's Seventh Framework Programme (FP/2007-2013)/ERC Grant, Agreement No. 279632.

REFERENCES

(1) Tahmasebpoor, M.; de Martin, L.; Talebi, M.; Mostoufi, N.; van Ommen, J. R. The role of the hydrogen bond in dense nanoparticle-gas suspensions. *Phys. Chem. Chem. Phys.* **2013**, *15*, 5788−5793.

(2) van Ommen, J. R.; Valverde, J.; Pfeffer, R. Fluidization of nanopowders: a review. *J. Nanopart. Res.* **2012**, *14*, 1−29.

(3) Li, J. F.; Huang, Y. F.; Ding, Y.; Yang, Z. L.; Li, S. B.; Zhou, X. S.; Fan, F. R.; Zhang, W.; Zhou, Z. Y.; Wu, D. Y.; Ren, B.; Wang, Z. L.; Tian, Z. Q. Shell-isolated nanoparticle-enhanced Raman spectroscopy. *Nature* **2010**, *464*, 392−395.

(4) Zhang, J.; Liu, P.; Lu, Z.; Xu, G.; Wang, X.; Qian, L.; Wang, H.; Zhang, E.; Xi, J.; Ji, Z. One-step synthesis of rutile nano-TiO_2 with exposed {111} facets for high photocatalytic activity. *J. Alloys Compd.* **2015**, *632*, 133−139.

(5) Daumann, B.; Weber, J. A.; Anlauf, H.; Nirschl, H. Discontinuous powder mixing of nanoscale particles. *Chem. Eng. J.* **2011**, *167*, 377−387.

(6) Balazs, A. C.; Emrick, T.; Russell, T. P. Nanoparticle Polymer Composites: Where Two Small Worlds Meet. *Science* **2006**, *314*, 1107−1110.

(7) Mädler, L.; Roessler, A.; Pratsinis, S. E.; Sahm, T.; Gurlo, A.; Barsan, N.; Weimar, U. Direct formation of highly porous gas-sensing films by in situ thermophoretic deposition of flame-made Pt/SnO_2 nanoparticles. *Sens. Actuators, B* **2006**, *114*, 283−295.

(8) Maver, U.; Znidarsic, A.; Gaberscek, M. An attempt to use atomic force microscopy for determination of bond type in lithium battery electrodes. *J. Mater. Chem.* **2011**, *21*, 4071−4075.

(9) Liong, M.; Lu, J.; Kovochich, M.; Xia, T.; Ruehm, S. G.; Nel, A. E.; Tamanoi, F.; Zink, J. I. Multifunctional Inorganic Nanoparticles for Imaging, Targeting, and Drug Delivery. *ACS Nano* **2008**, *2*, 889−896.

DOI: 10.1021/acs.langmuir.6b02982
Langmuir 2017, 33, 2477−2484

(10) Chithrani, B. D.; Ghazani, A. A.; Chan, W. C. W. Determining the Size and Shape Dependence of Gold Nanoparticle Uptake into Mammalian Cells. *Nano Lett.* **2006**, *6*, 662−668.
(11) Hu, L.; Wu, H.; La Mantia, F.; Yang, Y.; Cui, Y. Thin, Flexible Secondary Li-Ion Paper Batteries. *ACS Nano* **2010**, *4*, 5843−5848.
(12) Chen, X.; Mao, S. S. Titanium Dioxide Nanomaterials: Synthesis, Properties, Modifications, and Applications. *Chem. Rev.* **2007**, *107*, 2891−2959.
(13) Benn, T. M.; Westerhoff, P. Nanoparticle silver released into water from commercially available sock fabrics. *Environ. Sci. Technol.* **2008**, *42*, 4133−4139.
(14) Rumpf, H. Die Wissenschaft des Agglomerierens. *Chem. Ing. Tech.* **1974**, *46*, 1−11.
(15) Kammler, H. K.; Mädler, L.; Pratsinis, S. E. Flame Synthesis of Nanoparticles. *Chem. Eng. Technol.* **2001**, *24*, 583−596.
(16) Butt, H. J.; Kappl, M. *Surface and Interfacial Forces*, 1st ed.; Wiley-VCH, 2010.
(17) Israelachvili, J. N. *Intermolecular and Surface Forces*, 3rd ed.; Academic Press, 2011.
(18) Strobel, R.; Baiker, A.; Pratsinis, S. Aerosol flame synthesis of catalysts. *Adv. Powder Technol.* **2006**, *17*, 457−480.
(19) Teoh, W. Y.; Amal, R.; Mädler, L. Flame spray pyrolysis: An enabling technology for nanoparticles design and fabrication. *Nanoscale* **2010**, *2*, 1324−1347.
(20) Salameh, S.; Schneider, J.; Laube, J.; Alessandrini, A.; Facci, P.; Seo, J. W.; Colmbi Ciacchi, L.; Mädler, L. Adhesion Mechanisms of the Contact Interface of TiO_2 Nanoparticles in Films and Aggregates. *Langmuir* **2012**, *28*, 11457−11464.
(21) Xiao, X.; Qian, L. Investigation of Humidity-Dependent Capillary Force. *Langmuir* **2000**, *16*, 8153−8158.
(22) Hamaker, H. C. The London-van der Waals attraction between spherical particles. *Physica* **1937**, *4*, 1058−1072.
(23) Butt, H.-J.; Kappl, M. Normal capillary forces. *Adv. Colloid Interface Sci.* **2009**, *146*, 48−60.
(24) Horn, R. G.; Israelachvili, J. N. Direct measurement of structural forces between two surfaces in a nonpolar liquid. *J. Chem. Phys.* **1981**, *75*, 1400−1411.
(25) Cappella, B.; Baschieri, P.; Frediani, C.; Miccoli, P.; Ascoli, C. Force-distance curves by AFM. *IEEE Eng. Med. Biol.* **1997**, *16*, 58−65.
(26) Binnig, G.; Quate, C. F.; Gerber, C. Atomic force microscope. *Phys. Rev. Lett.* **1986**, *56*, 930−933.
(27) Kunze, C.; Giner, I.; Torun, B.; Grundmeier, G. Influence of the surface chemistry on TiO_2 − TiO_2 nanocontact forces as measured by an UHV−AFM. *Chem. Phys. Lett.* **2014**, *597*, 134−138.
(28) Farshchi-Tabrizi, M.; Kappl, M.; Cheng, Y. J.; Gutmann, J.; Butt, H. J. On the adhesion between fine particles and nanocontacts: An atomic force microscope study. *Langmuir* **2006**, *22*, 2171−2184.
(29) Thundat, T.; Zheng, X. Y.; Chen, G. Y.; Warmack, R. J. Role of relative humidity in atomic force microscopy imaging. *Surf. Sci.* **1993**, *294*, L939−L943.
(30) Butt, H.-J.; Farshchi-Tabrizi, M.; Kappl, M. Using capillary forces to determine the geometry of nanocontacts. *J. Appl. Phys.* **2006**, *100*, 024312.
(31) Weisenhorn, A. L.; Hansma, P. K.; Albrecht, T. R.; Quate, C. F. Forces in atomic force microscopy in air and water. *Appl. Phys. Lett.* **1989**, *54*, 2651−2653.
(32) Weisenhorn, A. L.; Maivald, P.; Butt, H. J.; Hansma, P. K. Measuring adhesion, attraction, and repulsion between surfaces in liquids with an atomic-force microscope. *Phys. Rev. B: Condens. Matter Mater. Phys.* **1992**, *45*, 11226.
(33) Dos Santos Ferreira, O.; Gelinck, E.; de Graaf, D.; Fischer, H. Adhesion experiments using an AFM-Parameters of influence. *Appl. Surf. Sci.* **2010**, *257*, 48−55.
(34) Kendall, K.; Rossetto, H.; Dhir, A.; Yong, C. W. Mechanics of Adhesion Through Nanolayers of Liquid. *J. Adhes.* **2012**, *88*, 108−117.
(35) Rong, W.; Pelling, A. E.; Ryan, A.; Gimzewski, J. K.; Friedlander, S. K. Complementary TEM and AFM Force Spectroscopy to Characterize the Nanomechanical Properties of Nanoparticle Chain Aggregates. *Nano Lett.* **2004**, *4*, 2287−2292.
(36) Rong Ding, W.; Mädler, L.; Ruoff, R. S.; Friedlander, S. K. Mechanical Properties of Nanoparticle Chain Aggregates by Combined AFM and SEM: Isolated Aggregates and Networks. *Nano Lett.* **2006**, *6*, 2646−2655.
(37) Laube, J.; Salameh, S.; Kappl, M.; Mädler, L.; Colombi Ciacchi, L. Contact Forces between TiO_2 Nanoparticles Governed by an Interplay of Adsorbed Water Layers and Roughness. *Langmuir* **2015**, *31*, 11288−11295.
(38) Salameh, S.; Scholz, R.; Seo, J. W.; Mädler, L. Contact behavior of size fractionated TiO_2 nanoparticle agglomerates and aggregates. *Powder Technol.* **2014**, *256*, 345−351.
(39) Fabre, A.; Salameh, S.; Ciacchi, L. C.; Kreutzer, M. T.; van Ommen, J. R. Contact mechanics of highly porous oxide nanoparticle agglomerates. *J. Nanopart. Res.* **2016**, *18*, 1−13.
(40) Panz, C. D.; Schmoll, R. D.; Kempf, M.; Scholz, M. D. *Hydrophobe, nicht getemperte Fällungskieselsäure mit hohem Weissgrad*; Degussa GmbH, 2007.
(41) Mueller, R.; Kammler, H. K.; Wegner, K.; Pratsinis, S. E. OH Surface Density of SiO_2 and TiO_2 by Thermogravimetric Analysis. *Langmuir* **2003**, *19*, 160−165.
(42) Hutter, J. L.; Bechhoefer, J. Calibration of atomic force microscope tips. *Rev. Sci. Instrum.* **1993**, *64*, 1868−1873.
(43) Friedlander, S. K. *Smoke, Dust, and Haze: Fundamentals of Aerosol Dynamics*; Oxford University Press, 2000.
(44) Derr, L.; Hildebrand, N.; Köppen, S.; Kunze, S.; Treccani, L.; Dringen, R.; Rezwan, K.; Colombi Ciacchi, L. Physisorption of α-chymotrypsin on SiO_2 and TiO_2: A comparative study via experiments and molecular dynamics simulations. *Biointerphases* **2016**, *11*, 011007.
(45) Erdem, B.; Hunsicker, R. A.; Simmons, G. W.; Sudol, E. D.; Dimonie, V. L.; El-Aasser, M. S. XPS and FTIR Surface Characterization of TiO_2 Particles Used in Polymer Encapsulation. *Langmuir* **2001**, *17*, 2664−2669.
(46) Kim, B. I.; Boehm, R. D.; Bonander, J. R. Direct observation of self-assembled chain-like water structures in a nanoscopic water meniscus. *J. Chem. Phys.* **2013**, *139*, 054701.
(47) Kim, B. I.; Rasmussen, J. A.; Kim, E. J. Large oscillatory forces generated by interfacial water under lateral modulation between two hydrophilic surfaces. *Appl. Phys. Lett.* **2011**, *99*, 201902.
(48) Choe, H.; Hong, M. H.; Seo, Y.; Lee, K.; Kim, G.; Cho, Y.; Ihm, J.; Jhe, W. Formation, Manipulation, and Elasticity Measurement of a Nanometric Column of Water Molecules. *Phys. Rev. Lett.* **2005**, *95*, 187801.
(49) Chiba, K.; Ohmori, R.; Tanigawa, H.; Yoneoka, T.; Tanaka, S. H2O trapping on various materials studied by AFM and XPS. *Fusion Eng. Des.* **2000**, *49*−*50*, 791−797.
(50) Bishop Kyle, J. M.; Wilmer, C. E.; Soh, S.; Grzybowski, B. A. Nanoscale Forces and Their Uses in Self-Assembly. *Small* **2009**, *5*, 1600−1630.
(51) Rance, G. A.; Marsh, D. H.; Bourne, S. J.; Reade, T. J.; Khlobystov, A. N. van der Waals Interactions between Nanotubes and Nanoparticles for Controlled Assembly of Composite Nanostructures. *ACS Nano* **2010**, *4*, 4920−4928.
(52) Ackler, H. D.; French, R. H.; Chiang, Y.-M. Comparisons of Hamaker Constants for Ceramic Systems with Intervening Vacuum or Water: From Force Laws and Physical Properties. *J. Colloid Interface Sci.* **1996**, *179*, 460−469.
(53) Bergström, L. Hamaker constants of inorganic materials. *Adv. Colloid Interface Sci.* **1997**, *70*, 125−169.
(54) Bertrand, F.; German, S.-A.; Anwar, A.; Irune, V.; Gemma, B.; Yolanda, R. D. M.; Lennart, B. Dispersion and surface functionalization of oxide nanoparticles for transparent photocatalytic and sunscreens. *Sci. Technol. Adv. Mater.* **2013**, *14*, 023001−023023.
(55) Dörmann, M.; Schmid, H.-J. Simulation of Capillary Bridges between Particles. *Procedia Eng.* **2015**, *102*, 14−23.
(56) Arnaudov, L. N.; Cayre, O. J.; Cohen Stuart, M. A.; Stoyanov, S. D.; Paunov, V. N. Measuring the three-phase contact angle of nanoparticles at fluid interfaces. *Phys. Chem. Chem. Phys.* **2010**, *12*, 328−331.

DOI: 10.1021/acs.langmuir.6b02982
Langmuir 2017, 33, 2477−2484

(57) Deak, A.; Hild, E.; Kovacs, A. L.; Horvolgyi, Z. Contact angle determination of nanoparticles: film balance and scanning angle reflectometry studies. *Phys. Chem. Chem. Phys.* **2007**, *9*, 6359−6370.
(58) Livadaru, L.; Kovalenko, A. The role of capillary and surface forces in the crossover behavior of solid nanoparticles at liquid interfaces. *J. Colloid Interface Sci.* **2006**, *304*, 254−260.

DOI: 10.1021/acs.langmuir.6b02982
Langmuir 2017, 33, 2477−2484